

A high-precision rf trap with minimized micromotion for an In^+ multiple-ion clock

K Pyka, N Herschbach, J Keller and T E Mehlstäubler

Physikalisch-Technische Bundesanstalt, Bundesallee 100, D-38116 Braunschweig, Germany

E-mail: karsten.pyka@ptb.de, tanja.mehlstaebler@ptb.de

Abstract.

We present an experiment to characterize our new linear ion trap designed for the operation of a many-ion optical clock using $^{115}\text{In}^+$ as clock ions. For the characterization of the trap as well as the sympathetic cooling of the clock ions we use $^{172}\text{Yb}^+$. The trap design has been derived from finite element method (FEM) calculations and a first prototype based on glass-reinforced thermoset laminates was built. This paper details on the trap manufacturing process and micromotion measurement. Excess micromotion is measured using photon-correlation spectroscopy with a resolution of 1.1 nm in motional amplitude, and residual axial rf fields in this trap are compared to FEM calculations. With this method, we demonstrate a sensitivity to systematic clock shifts due to excess micromotion of $|(\Delta\nu/\nu)_{\text{mm}}| = 8.5 \times 10^{-20}$. Based on the measurement of axial rf fields of our trap, we estimate a number of twelve ions that can be stored per trapping segment and used as an optical frequency standard with a fractional inaccuracy of $\leq 1 \times 10^{-18}$ due to micromotion.

Submitted to: *New J. Phys.*

Contents

1	Introduction	2
2	Experimental setup	3
2.1	Laser systems for the trapping of $^{172}\text{Yb}^+$	3
2.2	Experimental apparatus and detection scheme	5
3	The ion trap	8
3.1	Specifications	8
3.2	Trap fabrication	10
4	Characterization of the prototype trap	12
4.1	Trap operation	12
4.2	Photon-correlation spectroscopy	12
4.3	3D micromotion measurement in the trap	15
5	Conclusion	17

1. Introduction

The improvement of optical clocks based on single-ion spectroscopy has lead to frequency comparisons with a relative inaccuracy of $|\Delta\nu/\nu| < 1 \times 10^{-17}$ in the last years [1]. Most promising candidates have shown to be two-species systems, in which the clock ion is sympathetically cooled and the detection is realized through quantum logic spectroscopy [2]. To reduce systematic shifts related to excess micromotion for such a two-ion system, linear Paul traps are used, ideally having zero axial micromotion due to their geometry.

While single-ion clocks show an excellent potential to reach lowest frequency inaccuracy, they are limited in their short-term stability by the intrinsically low signal-to-noise ratio (SNR), as only one ion contributes to the clock signal. One approach to improve the short-term stability of the clock measurement, thus reducing lengthy averaging times, is to increase the spectroscopy pulse time on long-lived atomic states [1, 3]. This naturally limits the number of available clock ion candidates and places severe requirements on the clock laser stability.

Proposals have been made to develop an optical frequency standard based on many ions with increased SNR [4, 5]. In our approach, we sympathetically cool indium ions with ytterbium ions. Here, the direct spectroscopy of indium as the clock ion avoids quantum logic and facilitates scaling-up the clock read-out of many ions [4].

However, with a larger number of clock ions the residual axial micromotion of a linear ion trap and its associated systematic frequency shifts becomes an issue. In [1], for example, clock ion and cooling ion are separated by a distance of $3\text{ }\mu\text{m}$ along the trap axis. A relative frequency shift due to axial micromotion of $(\Delta\nu/\nu)_{\text{mm}} \approx -2.7 \times 10^{-17}$

is observed, when the ions swap their position. For an optical clock with many ions, it is a primary goal to engineer trap structures capable of trapping linear chains of ions with lowest possible axial rf fields and a high-level control of the ion dynamics.

A great effort in scalable trap engineering has been already made in quantum information experiments with trapped ions ([6, 7, 8, 9, 10, 11, 12, 13, 14]). Here, fast ion transport is required and relevant time scales are in the millisecond regime or below, thus electrode dimensions are comparatively small. In [4] we proposed a design for a scalable linear ion trap for an optical clock, in which up to ten ions can be stored per trapping segment within the Lamb-Dicke regime. Since observed excess heating rates scale with the ion-electrode distance d like $\Delta E_{\text{heat}}/dt \propto d^{-4}$ [15, 16], the trap electrode dimensions were chosen to be of millimeter size, to reach long interrogation times, unlimited by the heating of the ion. A strong effort is put on optical access and precise dimensions of the trap segments to minimize axial rf fields to a level required for ultra-precise clock spectroscopy.

In this paper we present our new experimental setup for testing high-precision ion traps and demonstrate successful operation of a first prototype. The atomic system used to characterize the ion trap is $^{172}\text{Yb}^+$. The laser system for this ion, the vacuum system and the detection scheme are described in section 2. In section 3, the design and the fabrication process of the prototype trap are explained in detail. In the last section, we focus on high-resolution micromotion measurements and compare experimentally determined axial rf fields to FEM calculations of this trap. We demonstrate a sensitivity of photon-correlation spectroscopy to micromotion induced frequency shifts of $|(\Delta\nu/\nu)_{\text{mm}}| < 10^{-19}$. With this method, we evaluate our ion trap to be capable of trapping up to 12 ions along the trap axis for high-precision spectroscopy with a micromotion induced relative frequency inaccuracy below 1×10^{-18} .

2. Experimental setup

2.1. Laser systems for the trapping of $^{172}\text{Yb}^+$

The advantage of the even isotope $^{172}\text{Yb}^+$, used to characterize the ion trap, is the absence of a hyperfine structure and thus a low number of electronic states that have to be addressed. Four different diode lasers are used for photoionization, cooling and detection, and repumping. An overview of the relevant energy levels including their linewidth and transition wavelength is given in figure 1.

For photoionization, a frequency-doubled external cavity diode laser (ECDL) system is used to resonantly excite neutral ^{172}Yb to its $^1\text{P}_1$ state. A single pass through a Brewster-cut periodically-poled potassium titanyl phosphate (PPKTP) crystal is sufficient to generate a power of $P_{399\text{nm}} = 80\mu\text{W}$, out of which $7\mu\text{W}$ are sent to the atoms. The beam is guided through the trap vertically, whereas the atomic beam of neutral Yb passes horizontally through the trap. Thereby, Doppler-shifts and broadening due to the high temperature of the atoms are avoided. In fact, a scan of

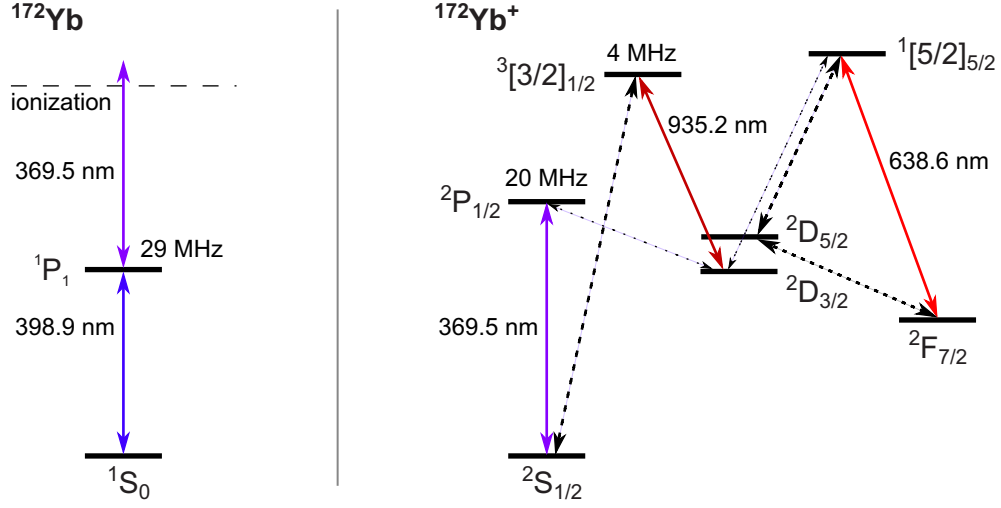


Figure 1. Left: Photoionization of ^{172}Yb via two-step laser excitation. Right: Partial level-scheme of $^{172}\text{Yb}^+$ with atomic transitions used for cooling and repumping.

the laser shows a full-width half maximum of only 35 MHz at a saturation parameter of $s = 2\Omega^2/\Gamma^2 \lesssim 1$, where Ω is the Rabi-frequency and Γ the decay rate of the excited state.

An optically amplified and frequency-doubled diode laser system (Toptica TA SHG pro) delivers an output power of $P_{369\text{nm}} = 55 \text{ mW}$ at a wavelength of 369.5 nm. This light is used to cool and detect the ions by driving the $^2\text{S}_{1/2} \leftrightarrow ^2\text{P}_{1/2}$ transition of $^{172}\text{Yb}^+$. It is also used for the second excitation step of the photoionization process. The laser is divided into three beams, all sent to the trap via polarization-maintaining optical fibers. All beams are collimated and imaged into the trap with a waist of $\omega_{369\text{nm}} = 80 \mu\text{m}$, where the cooling beam in the vertical direction is overlapped with the photoionization beam, see figure 3. The power used for Doppler cooling and detection of a single ion is $\approx 3 \mu\text{W}$, which gives a saturation parameter of $s_{369\text{nm}} = 0.6$ for each beam. In order to cool and perform spectroscopy on chains of ions in more than one trap segment simultaneously, it is necessary to expand the beams along the trap axis over several millimeters. This will be done in the near future and will make use of the high power provided by this laser.

Due to the decay channel from the cooling transition to the long-lived $^2\text{D}_{3/2}$ state, constant cooling of the ion is only possible by depleting the population of this dark state. Therefore, another laser beam with a power of 20 mW is sent to the ions, driving the $^2\text{D}_{3/2} \leftrightarrow ^3[3/2]_{1/2}$ transition at a wavelength of 935.2 nm. The beam is guided in a single-mode polarization-maintaining optical fiber and imaged with a $f = 500 \text{ mm}$ lens along the trap axis (Z, see figure 3), having a minimum waist of $\omega_{935\text{nm}} = 125 \mu\text{m}$ at the trap center.

Collisions with the background gas in the vacuum chamber can populate the metastable $^2\text{F}_{7/2}$ state by a combination of non-radiative and radiative decays [17]. This state has an estimated lifetime of several years [3, 18], so the ion is lost for

the experimental sequence and the decoupling from the cooling-cycle leads to heating and eventual loss from the trap. Also, quenching of the metastable state population via collisions with heavier background molecules such as H_2O is observed. For a deterministic clean-out of the $^2\text{F}_{7/2}$ state, a second repump laser at 638.6 nm is used in the experiment. About 5.5 mW of this light is overlapped with the 935.2 nm laser beam, again having a waist of $\omega_{639\text{nm}} = 125 \mu\text{m}$ at the trap center.

A wavelength meter based on a Fizeau interferometer[†] with an 8-channel multi-mode fiber switch serves as a frequency reference for all lasers. The specified absolute frequency accuracy is 60 MHz in a range of 350 nm to 1100 nm for a single-mode fiber connection, and 200 MHz for the multi-channel switch operation. Slow frequency drifts of the diode lasers are compensated with an electronic feedback on their piezo actuators by our experiment control software. The reproducibility of the measured frequencies is about 1 MHz from shot to shot. With a temperature stability of $\sigma_T = 0.2 \text{ K/h}$ a drift of less than 3 MHz per hour is observed. Figure 2 shows the stability of the wavemeter read-out against an ultra-stable laser with a sub-Hz linewidth and a few 100 mHz/s drift.

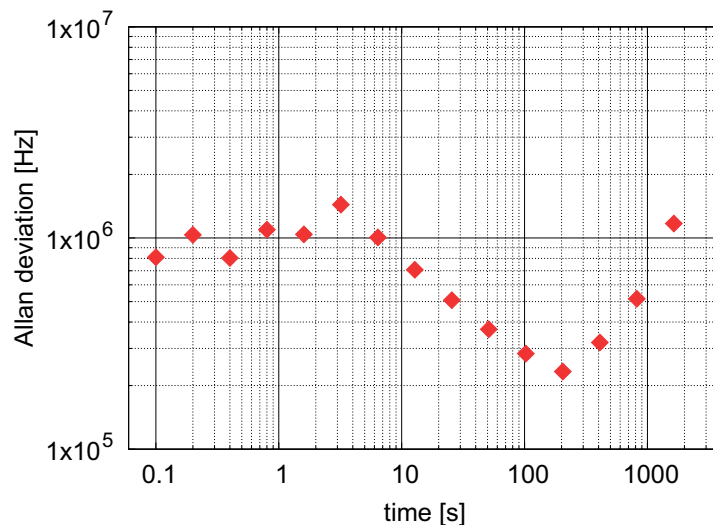


Figure 2. Temporal stability of the wavemeter read-out. Shown is the Allan deviation of a typical frequency measurement of our stable reference laser at 822 nm, with sub-Hz linewidth and drift of $< 1 \text{ Hz/s}$, using the WS-7 wavemeter.

2.2. Experimental apparatus and detection scheme

The vacuum system is designed for testing and characterization of different trap geometries and provides versatile optical and electrical access. The cylindrical chamber is based on a DN250 flange with adapter flanges on the side and bottom for windows and electrical feedthroughs.

[†] High Finesse, WS-7

Six windows are mounted pairwise in the horizontal plane and allow laser beams to pass along the trap axis (Z) as well as under an angle of $\theta = \pm 25^\circ$ to the z-axis (H1 and H2). One vertical laser beam (V) passes perpendicularly to the horizontal plane through the ion trap. With this setup, we are able to measure excess micromotion of the ion in all three dimensions and characterize the trap. A detailed scheme is shown in figure 3.

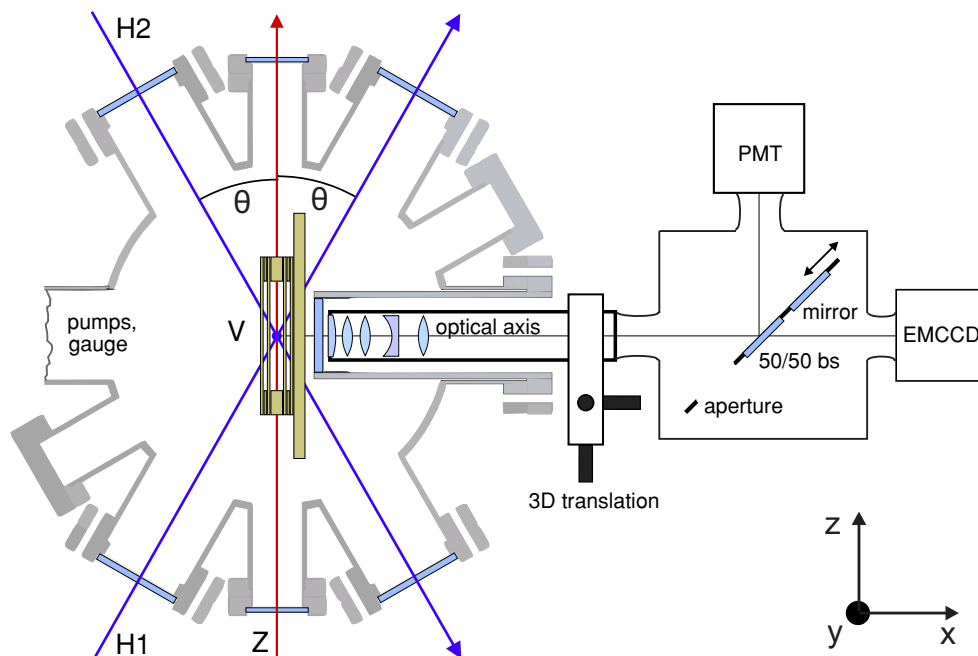


Figure 3. Schematic top view of the experimental setup. The trap is placed in front of the re-entrant vacuum viewport. Three laser beams (**H1**, **H2**, **V**) at 369.5 nm are used for the measurement of micromotion in all spatial dimensions. Laser beams along **Z** provide light at 638.5 nm and 935.2 nm for repumping. The photoionization laser at 398.9 nm is overlapped with the beam in y direction.

For detection, a re-entrant viewport is mounted horizontally and perpendicularly to the trap axis with a distance of 23 mm between the vacuum window and the trap center. A self-built lens system with standard spherical 1 inch lenses and a working distance of 37 mm provides a light collection efficiency of 2 %. The lens design is a retrofocus lens with a numerical aperture $NA = 0.27$. In order to assure wavefront errors smaller than $\lambda/4$ the lens positions have been optimized with a commercial ray-tracing software. With a magnification $V = 25$ and a CCD-chip pixel size of $16 \mu\text{m}$, we obtain a spatial resolution of $0.6 \mu\text{m}/\text{px}$ on our camera.

The detection scheme is twofold: it is possible to either detect with the electron multiplying CCD (EMCCD) camera[‡] or with a photomultiplier[§] (PMT). Also, it is possible to detect ions with both devices simultaneously using a 50/50 beam splitter. The latter configuration was used during the measurements presented in this paper.

[‡] Andor: DU-897, $512 \text{ px} \times 512 \text{ px}$, quantum efficiency $QE = 35 \%$ for 200 nm – 370 nm

[§] Hamamatsu: R7207-01, Bialkali window, $QE \geq 20 \%$ for 160 nm – 650 nm

The vacuum in the apparatus is maintained by an ion getter pump, having a nominal pumping speed of 20 mbar l/s for air and a titanium sublimation pump in a DN63 tube, with a calculated pumping speed of 490 mbar l/s for hydrogen. The residual pressure after pre-baking, re-opening and inserting the ion trap, followed by a modest bake-out at 60 °C is 1.0×10^{-8} Pa.

An 8-pole feedthrough provides a high current connection to the Yb and In ovens inside the vacuum chamber. The oven design consists of a vertical tantalum tube with an outer diameter of 1.02 mm and an inner diameter of 0.86 mm. On both ends, copper wires are spot-welded to provide the heating current. A 0.4 mm diameter hole on the side of the tantalum tube generates an atomic beam. To collimate the atomic beams of both ovens, a copper shield with two slits of ≈ 1 mm in the horizontal direction is placed between the ovens and the trap, assuring atomic flux through the loading segment, while the spectroscopy segments do not get contaminated. An isotope-enriched sample of ytterbium is used, as the natural abundance of the isotopes ^{172}Yb and ^{173}Yb are 22 % and 16 %, respectively. Their photoionization resonances are separated by only 55 MHz and show considerable overlap. A frequency scan of the photoionization laser is shown in figure 4.

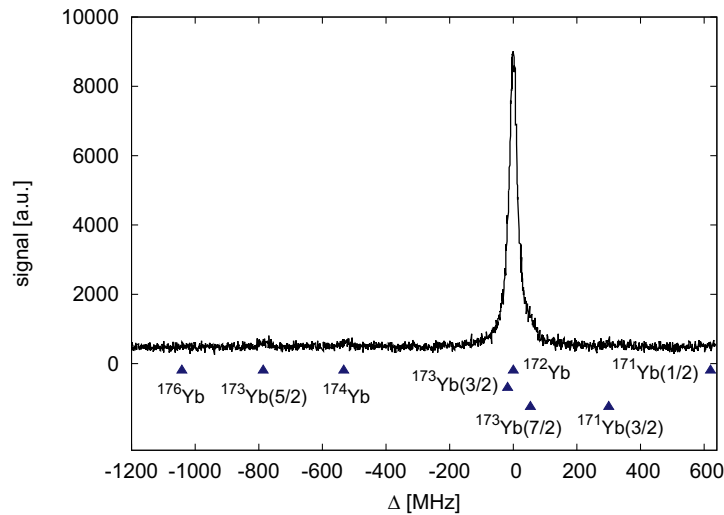


Figure 4. 399 nm laser scan with isotope enriched ^{172}Yb sample. The expected resonances of the various isotopes [19] are indicated by triangles.

A 41-pole feedthrough provides the connection for the various dc voltages for axial confinement of the ions and for micromotion compensation in our segmented linear Paul trap. The dc voltages are generated by a 13 bit analog output PCI-card^{||}. A self-built low-pass filter and a distribution box combine the axial confinement voltages and radial compensation voltages that are applied on a common trap electrode. A detailed scheme is shown in figure 6. For the electrodes with strongest passage, the compensation voltages provided by the PCI-card are divided down to improve the resolution of the

^{||} National Instruments: NI 6723 with 32 analog outputs

field, which is applied to shift the ions in the radial direction (U_{tc}). The range and resolution of all three fields are summed up in table 1.

Furthermore, an HN type coaxial feedthrough connects the trap with the helical resonator, which generates the high-voltage rf field for the radial confinement, that is necessary in order to achieve high secular frequencies for $^{172}\text{Yb}^+$. To reduce heating of the system due to power dissipation, the resonator is designed for a high quality factor according to [20]. With a free-standing coil, made of a 5 mm thick copper wire, an unloaded quality factor of $Q_{\text{unloaded}} = 1050$ has been realized. Connected to the trap, the quality factor is $Q_{\text{loaded}} = 640$ and the resonance frequency for driving the trap is $\Omega_{\text{rf}} = 2\pi \times 25.67 \text{ MHz}$. The amplitude of the rf voltage is measured by a calibrated thin wire pick-up, which is placed inside the helical resonator tank. A schematic drawing of the resonator is given in figure 5.

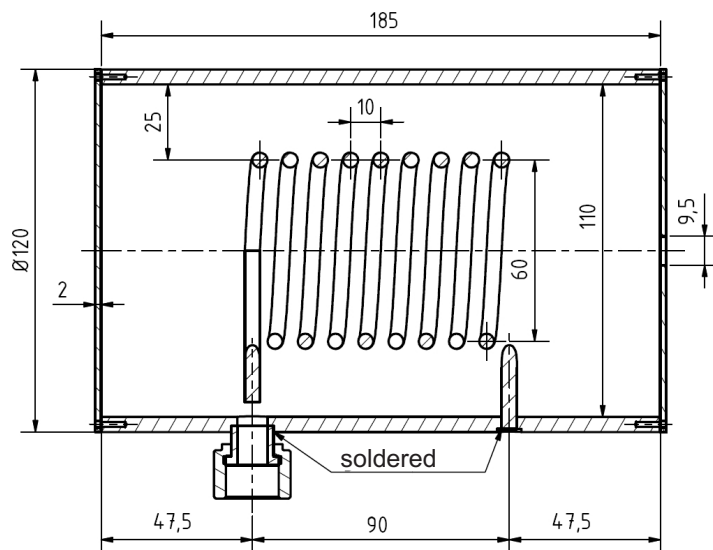


Figure 5. Schematic drawing of the helical resonator for rf voltage generation in our setup. All dimensions are given in mm. The resonator coil is made of 5 mm thick Cu wire. The circuit is fed from the right side by a primary coil with a single winding, not shown in the drawing. Connected to the trap load of 16 pF, we achieve a quality factor of $Q_{\text{loaded}} = 640$.

With this system, the ion trap can be driven with an rf voltage amplitude of 1500 V using an rf power $< 2 \text{ W}$.

3. The ion trap

3.1. Specifications

The trap introduced in this paper is based on a design published in [4]. The main goal is to obtain a scalable structure of an array of linear Paul traps, where chains of about 10 ions can be stored in the Lamb-Dicke regime in each trapping segment, with axial rf fields at negligible level. This means micromotion induced systematic fractional

frequency shifts need to be below 1×10^{-18} . For this, FEM calculations had been carried out to estimate the effects of alignment uncertainties and machining tolerances on the rf potential. In order to test the trap design and the new experimental setup, a simplified prototype trap has been built from easily machinable thermoset wafers, featuring one loading segment and two spectroscopy segments. The realized electrode structure with five electronically isolated segments and the geometric dimensions are shown in figure 6.

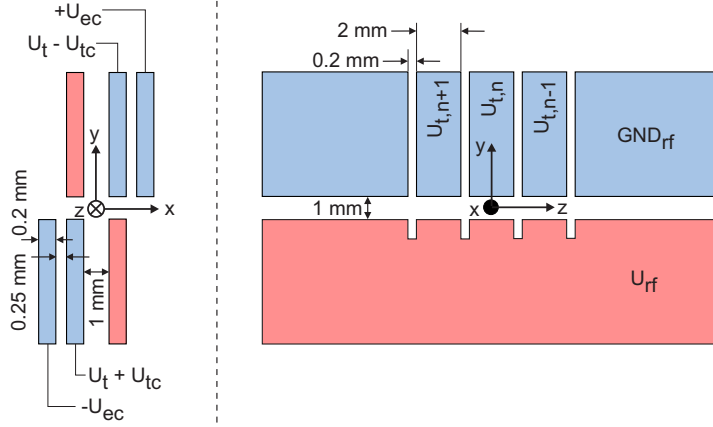


Figure 6. Trap geometry and electronic configuration. All rf ground electrode segments are dc isolated from each other. With individual voltages $U_{t,n}$ axial confinement is realized. A differential voltage $U_{tc,n}$ provides compensation fields in radially diagonal direction in each segment n . A differential voltage $U_{ec,n}$ on the outer compensation electrodes provides an independent second field vector to move the ions to any position in the xy-plane.

The rf electrodes U_{rf} only carry the high rf voltage for the radial confinement of the ions, whereas the rf ground electrodes GND_{rf} provide dc voltages for the axial confinement of the ions as well as the micromotion compensation in all three dimensions. The inner electrodes opposite to the rf electrodes are used for axial confinement as well as micromotion compensation, while the outer electrodes are used for micromotion compensation only. Table 1 shows the dc voltages that can be applied, together with their resolution and the corresponding dc electric field calculated at the position of the ion.

For the axial confinement, U_t is applied to the electrodes neighbouring the used trap segment. A typical value for most measurements presented in this paper is $\omega_{ax,Yb} = 2\pi \times 116 \text{ kHz}$ at $U_{t,n-1} = U_{t,n+1} = 4 \text{ V}$ and $U_{t,n} = 0 \text{ V}$. As those electrodes are controlled independently, they can also be used for micromotion compensation as well as shifting the ion along the trap axis to measure residual rf electric fields. Here, a field resolution of $\Delta E_{z,min} = 0.30 \text{ V/m}$ corresponds to a spatial shift of $0.3 \mu\text{m}$ at $\omega_{ax,Yb} = 2\pi \times 116 \text{ kHz}$.

For micromotion compensation in radial direction, U_{ec} and U_{tc} are used. U_{ec} generates a field, which has its strongest vector component (90%) along the x-axis and is solely used to shift the ion along this direction. U_{tc} generates a field with strong

Table 1. DC voltages that can be applied to the trap electrodes. The corresponding maximum electric field at the position of the ions and its resolution is given along the specified trap axis.

	trap axis	ΔU_{dc}	$U_{\text{dc,range}}$	ΔE_{dc}	$E_{\text{dc,range}}$
U_{tc}	x	0.6 mV	± 2.5 V	0.32 V/m	1325 V/m
	y			0.40 V/m	1650 V/m
U_{ec}	x	2.9 mV	± 12 V	0.45 V/m	1860 V/m
	y			0.05 V/m	204 V/m
U_{t}	z	2.9 mV	± 12 V	0.30 V/m	612 V/m

components in both x and y direction, which makes it necessary to compensate with U_{ec} in x direction when shifting the ion along the y-axis. The equally spaced quadrupole electrode geometry leads to an efficient rf trapping potential in radial direction with a calculated loss factor of $L = 1.29$ [21].

For clock operation, radial secular frequencies of more than 1 MHz can be reached with indium ions at an rf trap voltage of 1500 V. For the trap characterization with $^{172}\text{Yb}^+$, a lower rf voltage amplitude of $U_{\text{rf}} = 810$ V is used, resulting in radial secular frequencies of $\omega_{\text{rad,Yb}} = 2\pi \times 484$ kHz. At this rf amplitude the trap depth is 2.2 eV in x direction and 3.4 eV in y direction. The principal axes of the trap are rotated with respect to the x-axis by about 36° and 126° .

3.2. Trap fabrication

The prototype ion trap is made of Rogers4350BTM, a glass-reinforced, ceramic-filled hydrocarbon thermoset with low rf losses ($\tan \delta < 0.0037$)¶. This makes it possible to generate a high trapping rf voltage with low input power. The electrodes are made of laser structured 200 μm thick wafers, with a 35 μm conductive copper layer and a 10 μm gold thick-film. A thin nickel layer is used as an adhesion promoter.

Four boards are stacked on top of each other and mounted on a carrier board as shown in figure 7. Two identical boards (1), one of which is rotated by 180° around the trap axis relative to the other, form the quadrupole trap. They are separated by four 1 mm thick spacers placed in the corners. An additional board (2) is attached on top of each of the trap boards, with spacers of 0.25 mm thickness. The stack is glued on a 1.5 mm thick carrier board (3), which provides gold pins as dc voltage connectors to the multipin feedthrough and a mount for the rf connection. The rf lead is a 0.1 mm thick, oxygen-free copper foil cut into 5 mm wide strips of equal length to avoid phase shifts on the rf electrodes.

To prevent coupling of rf power into the dc voltage sources as well as coupling of high-frequency noise onto the trap electrodes, low-pass filters are mounted directly on the trap boards close to the dc electrodes. Non-magnetic and UHV-proof SMD

¶ see <http://www.rogerscorp.com>, not available anymore, but current 4360 shows same specifications

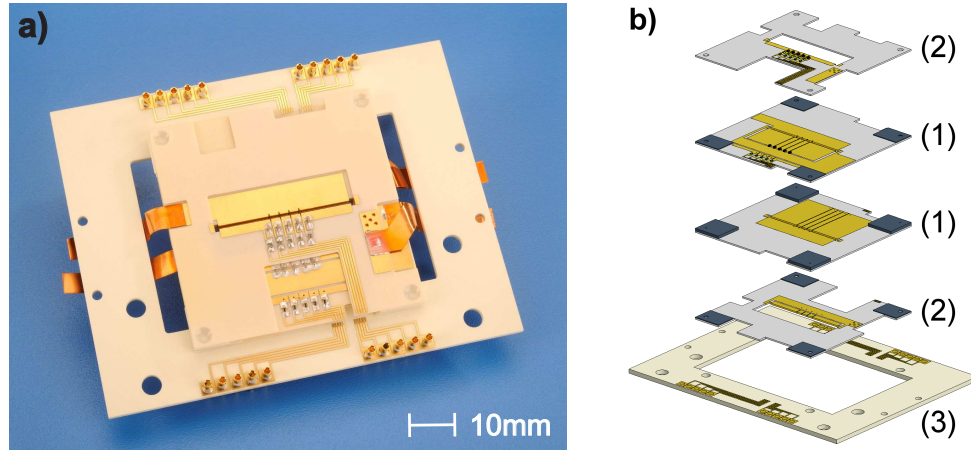


Figure 7. a) Photograph of the assembled trap stack with on-board filter electronics, connector pins for dc voltages on the carrier board and rf feed copper strips. b) Scheme of the trap assembly with two trap (1) and two compensation (2) boards with spacers (dark grey) on the corners to provide optical access for the laser beams.

components⁺ are soldered with a lead free UHV compatible solder*. The copper foil strips used for the rf connection are soldered onto the boards as well.

After fitting all boards with the electrical components, they were aligned under the cross-hair of a microscope[‡]. Translation stages with a $1\text{ }\mu\text{m}$ scale and a rotation stage with a 1 arcsecond scale provided high-precision alignment control. The boards were fixed one after the other using a glue with low outgassing and low shrinkage^{††}. This glue has the advantage of being both heat and UV curable. After stabilizing the boards with a broadband UV lamp, the complete stack was heated in an oven for 30 min at 130°C to ensure that all glue was cured. The dc leads on the individual electrode boards were then connected to the carrier board with a ball bonder using $30\text{ }\mu\text{m}$ thick gold wires. Finally, the gold pins were soldered to the carrier board for the dc voltage connection. The link to the vacuum feedthrough is made with Kapton coated wires with crimped connectors.

As a first check, the magnetization of the single components of the trap was measured with a fluxgate in a μ -metal box with a sensitivity of $\leq 100\text{ nT}$. No effect could be measured for either the SMD parts or the trap boards. Apparently, the thin nickel layer used as an adhesion promoter does not show bulk behavior yet and therefore no ferromagnetic properties. Only for the gold-plated pins for the dc voltage connection a residual magnetization of about $1\text{ }\mu\text{T}$ at a probe distance of 7 mm could be measured. Scanning the probe over the trap stack, field amplitudes of up to $2\text{ }\mu\text{T}$ were measured near the pins at the edge of the carrier board, but no field was resolved in the vicinity

⁺ Resistors: $R = 300\text{ k}\Omega$, Barry Industries - partnumber: RP0402BA-3003 JN-91. Capacitors: $C = 4.7\text{ nF}$, Novacap - partnumber: 0402 C472 J500 PH-HB. Low-pass cutoff frequency: $\nu_{\text{cutoff}} = 113\text{ Hz}$

* Kester: 80Sn19Ag1Cu

[‡] Leitz UWM

^{††} Optocast 3410 Gen2, see <http://outgassing.nasa.gov/> for vacuum compatibility

of the trap slit. For the final trap design, the gold pins will be replaced by soldered dc connections on the carrier board.

4. Characterization of the prototype trap

4.1. Trap operation

As a first test of the ovens and the ion trap, a single lens was used to observe the whole trapping region. The fluorescence of neutral Yb atoms was observed in the trace of the photoionization beam passing through the loading segment, segment 3 in figure 8. By moving the laser beam through all trap segments and detecting atoms only in segment 3, we were able to verify the alignment of the atomic beam aperture. Ions were loaded and shuttled into all three trap segments. With our self-built detection lens the magnification was then increased to $V = 25$, which leads to a resolution of $\approx 0.6 \mu\text{m}/\text{px}$ and makes it possible to resolve single ions in a Coulomb crystal in one trap segment, see figure 8. Deterministic loading of single ions was demonstrated.

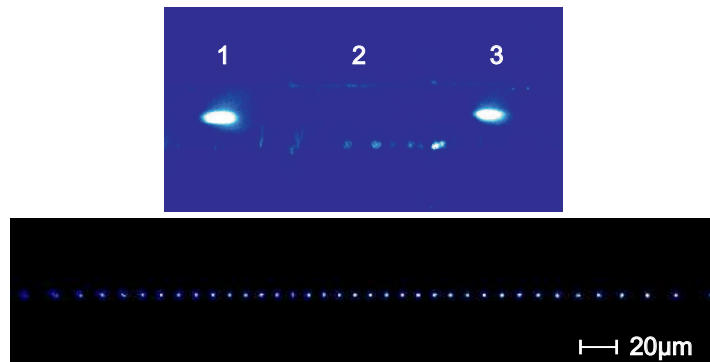


Figure 8. Top: trapping and shuttling of $^{172}\text{Yb}^+$ ions in ion trap, illuminated by beams of the cooling laser along H1 and H2. The stray light of the laser beams makes the segmented trap structure visible. Bottom: picture of a linear Coulomb crystal of 37 $^{172}\text{Yb}^+$ ions, trapped in segment 3 and imaged with the self-built diffraction limited lens.

The radial secular frequencies were measured for a single $^{172}\text{Yb}^+$ ion by amplitude modulation of the rf electric field. For an rf voltage amplitude of $U_{\text{rf}} = 810 \text{ V}$ and a dc voltage $U_t = 0.05 \text{ V}$, two radial secular frequencies of $\omega_{\text{rad},1} = 2\pi \times 490 \text{ kHz}$ and $\omega_{\text{rad},2} = 2\pi \times 472 \text{ kHz}$ were measured. Here, the rf voltage is deduced from the calibrated pick-up voltage U_{mon} of the helical resonator with $K = U_{\text{rf}}/U_{\text{mon}} = 5400 \pm 340$. The observed trap frequencies are, within a few percent, in good agreement with the calculated rf potential.

4.2. Photon-correlation spectroscopy

A single $^{172}\text{Yb}^+$ ion is loaded into the trap to measure residual micromotion in our trap by photon-correlation spectroscopy. This technique measures the rf field induced motion

of the ion via its 1st order Doppler-shift on a broad atomic line with linewidth Γ . In order to resolve the weak modulation of the ion fluorescence at the trap frequency, its scattering rate is correlated with the phase of the rf trap voltage. A time-to-amplitude-converter (TAC) generates pulses with a height dependent on the time T between a START-signal, triggered by the detection of a photon by the PMT, and a STOP-signal generated by the rf voltage of the trap. A multi-channel-analyzer yields a histogram of these pulses sorted in height and thus, in time difference T . Thereby, the modulation amplitude of the ion's fluorescence at the trap frequency Ω_{rf} is observed. A detailed description of the method can be found in [22].

As an example, figure 9 shows the histograms of two measurements of the radial micromotion component along the y-axis of a single ion as measured by the laser beam along V. For each measurement, the data acquisition time is 30 s. In the measurement

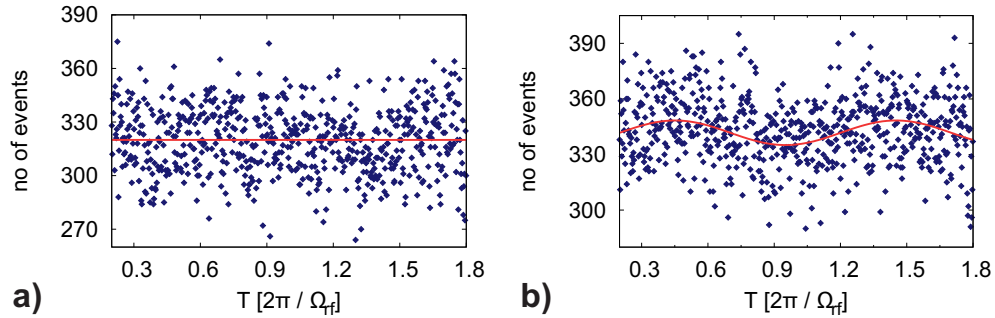


Figure 9. Photon-correlation signal of micromotion along y direction as measured with vertical laser beam (V). The acquisition time is 30 s. a) Ion with optimized micromotion. Restricting the phase to $-\pi/2 < \varphi_{\text{mm}} < \pi/2$ the fit yields $S_{\text{mod}}/S_{\text{max}} = 0 \pm 0.0017$. b) Ion shifted by $\Delta U_{\text{ec}} = 5.8 \text{ mV}$ (corresponding to $\Delta x = 57 \text{ nm}$) in x direction. The red line is a sine fit to the data with $S_{\text{mod}}/S_{\text{max}} = 0.011$.

shown in figure 9, where micromotion is detected along the vertical laser beam, a weak laser beam along H1 is present to cool the ion in the axial direction. The average photon count rate at a detuning of $\omega_{\text{laser}} - \omega_{\text{ion}} = -\Gamma/2$ is about $10\,800 \text{ s}^{-1}$, including a background of about 1800 s^{-1} .

Using the laser beams in H1, H2 and V, respectively, the micromotion can be measured in all dimensions. The velocity amplitude of rf induced ion motion v_{mm} is evaluated using the linearization of the line profile, which is a valid approximation for $k v_{\text{mm}} \ll \Gamma$. In this case, the signal contribution $S_{\text{det},i}$ of each beam i can be written as

$$S_{\text{det},i} = \frac{S_{\text{max},i}}{2} + S_{\text{mod},i} \sin(\Omega_{\text{rf}}t + \varphi_{\text{mm},i}), \quad i=\text{H1,H2,V}, \quad (1)$$

where $S_{\text{max},i}/2$ is the ion's fluorescence at $\omega_{\text{laser}} - \omega_{\text{ion}} = -\Gamma/2$, which corresponds to half of the maximum fluorescence for a Lorentzian probability distribution. $S_{\text{mod},i}$ is the fluorescence modulation amplitude and $\varphi_{\text{mm},i}$ is the phase of the motion relative to the rf voltage. To improve the fit of the data, the frequency of the rf trigger signal is $\Omega_{\text{rf}}/2$, so that the data set contains two rf periods, i.e. $T = 0 \dots 4\pi/\Omega_{\text{rf}}$. From the individual measurements along laser beams H1, H2 and V, the velocity components along the trap

axes are extracted using:

$$\frac{k v_{\text{mm},y}}{\Gamma_{\text{nat}}} = \frac{S_{\text{mod},V} \sqrt{1 + s_V}}{S_{\text{max},V} f_c}, \quad (2)$$

$$\frac{k v_{\text{mm},x}}{\Gamma_{\text{nat}}} = \frac{1}{2 \cos \theta_x f_c} \cdot \sqrt{A^2 + B^2 + 2AB \cos(\varphi_{\text{H2}} - \varphi_{\text{H1}})} \quad \text{and} \quad (3)$$

$$\frac{k v_{\text{mm},z}}{\Gamma_{\text{nat}}} = \frac{1}{2 \cos \theta_z f_c} \cdot \sqrt{A^2 + B^2 - 2AB \cos(\varphi_{\text{H2}} - \varphi_{\text{H1}})}, \quad (4)$$

$$\text{with } A, B = \frac{S_{\text{mod,H1,H2}} \cdot \sqrt{1 + s_{\text{H1,H2}}}}{S_{\text{max,H1,H2}}}.$$

Here, $k = 2\pi/369.5 \text{ nm}$ and $\theta_x = 65^\circ$ and $\theta_z = 25^\circ$ are the projection angles of the laser beams H1 and H2 to the trap axes x and z, respectively. Saturation broadening of the atomic line is taken into account by the individual saturation parameters s_i of each laser beam.

In addition, the measured signal is corrected by a factor f_c , due to the finite lifetime of the excited state of the ion. Only when the lifetime of the excited state is much shorter than the modulation period of the signal ($\tau \ll T_{\text{rf}}$), the full signal amplitude $S_{\text{mod}}^{(0)}$ is observed. In general, the fluorescence of an ion, when excited by a periodic signal, follows the differential equation $\dot{S}(t) = \tau^{-1} S(t) + S_{\text{drive}}(t)$, with a periodic term $S_{\text{drive}}(t)$ [23]. The general solution to this equation is:

$$S(t) = e^{-t/\tau} \left(c_1 + \int_{-\infty}^t S_{\text{drive}}(t') e^{t'/\tau} dt' \right), \quad (5)$$

which consists of a fast exponential decay and the damped response to the modulation. For the fluorescence of a laser-cooled ion with micromotion, this modulation is $S_{\text{drive}}(t) = S_0 + S_{\text{mod}}^{(0)} \sin(\Omega_{\text{rf}} t)$, with $S_{\text{mod}}^{(0)} \propto |\mathbf{k} \cdot \mathbf{v}_{\text{mm}}|$. For times larger than the natural decay time τ , (5) gives:

$$\begin{aligned} S(t) &= \tau S_0 + S_{\text{mod}}^{(0)} \cdot \frac{\tau^{-1} \sin(\Omega_{\text{rf}} t) - \Omega_{\text{rf}} \cos(\Omega_{\text{rf}} t)}{\tau^{-2} + \Omega_{\text{rf}}^2}, \\ &= \tau S_0 + S_{\text{mod}}^{(0)} \cdot (\tau^{-2} + \Omega_{\text{rf}}^2)^{-1/2} \cdot \sin(\Omega_{\text{rf}} t + \varphi_i). \end{aligned} \quad (6)$$

From this the modulation m_{det} of the detected fluorescence is derived to be

$$m_{\text{det}} = \frac{S_{\text{mod}}^{(0)} \cdot (\tau^{-2} + \Omega_{\text{rf}}^2)^{-1/2}}{\tau S_0} = \frac{S_{\text{mod}}^{(0)}}{S_0} \cdot f_c, \quad (7)$$

giving a reduction in contrast compared to the modulation $m_0 = S_{\text{mod}}^{(0)}/S_0$ of

$$f_c = \frac{1}{\sqrt{1 + (\Omega_{\text{rf}} \tau)^2}}. \quad (8)$$

With a lifetime $\tau = 8 \text{ ns}$, this correction term amounts to $f_c = 0.61$.

The finite saturation parameter $s_i \approx 0.6$ of each laser beam leads to a reduction of the measured micromotion velocity amplitude of about 26 %. It is evaluated before the measurement by scanning the cooling laser over the resonance and fitting a Lorentzian profile to the scan. The fit gives the effective linewidth and hence the

saturation parameter for each laser beam with an uncertainty of about 8%, which is the major contribution to the systematic uncertainty of the data. Compared to that, the uncertainty in the angles of the laser beams to the trap axes are negligible and not taken into account.

Great care is taken to correctly subtract the background signal due to laser straylight from the fitted off-set $S_{\max,i}/2$. The detection laser itself contributes about 5 – 10% to the background. In the case of measuring micromotion along V, laser beam H1 is present during the measurement to compensate axial heating of the ion. For this purpose the power in beam H1 is reduced by a factor of 14 and no contribution to the modulation amplitude is detectable. Only a constant offset is subtracted from $S_{\max,V}/2$.

The resolution achieved in the measurements is limited in general by intensity and frequency fluctuations of the spectroscopy laser. This contribution has been evaluated from repetitive measurements in all laser beams. Due to the laser beam geometry, the highest sensitivity to rf fields of $\sigma_{\text{rf}} = 21 \text{ V/m}$ is reached for the micromotion y component measured along laser beam V. For the measurements along the trap axis this uncertainty is 22 V/m. The lowest sensitivity is obtained in x direction with $\sigma_{\text{rf}} = 49 \text{ V/m}$. The fit to the data contributes an additional uncertainty of 8 V/m.

As shown in figure 9, an electric field of $\Delta E_x = 0.9 \text{ V/m}$, corresponding to $\Delta U_{\text{ec}} = 5.8 \text{ mV}$, has to be applied to produce a detectable micromotion along the y-axis. This corresponds to an rf field amplitude of $E_{\text{rf},x} = (51 \pm 23) \text{ V/m}$, or an excess micromotion amplitude of 1.1 nm. With $(\Delta\nu/\nu)_{\text{mm}} = -v_{\text{mm}}^2/2c^2$, this gives a relative frequency shift due to time dilation of -8.5×10^{-20} . Here, the resolved rf field is limited only by the resolution of the dc voltage control on the electrodes that moves the ion radially.

4.3. 3D micromotion measurement in the trap

To characterize and test the photon-correlation method quantitatively, a single ion was first shifted in both radial directions of the trap, where the strong rf quadrupole potential dominates and its field gradients can be determined accurately from our measurements of the secular frequencies. In figure 10a the micromotion measurement is shown for an ion shifted along the y direction and in figure 10b for an ion shifted along the x direction. The graphs show the measured rf electric field component perpendicular to the direction of the ion shift as a function of the ion position in the trap. The position of the ion is calculated according to (16) in [22] using the measured radial secular frequencies and the calculated dc electric fields applied by changing U_{tc} and U_{ec} . For comparison, the rf electric field obtained by the FEM calculations is plotted together with the measured data as a function of the ion position.

The measurement of the y component of the field is in good agreement with the calculation, whereas the x component shows a deviation of about 25%. This can be explained by the fact, that the Rogers4350BTM boards are elastic. Pictures taken from the assembled trap stack show, that the outer compensation boards slightly bend

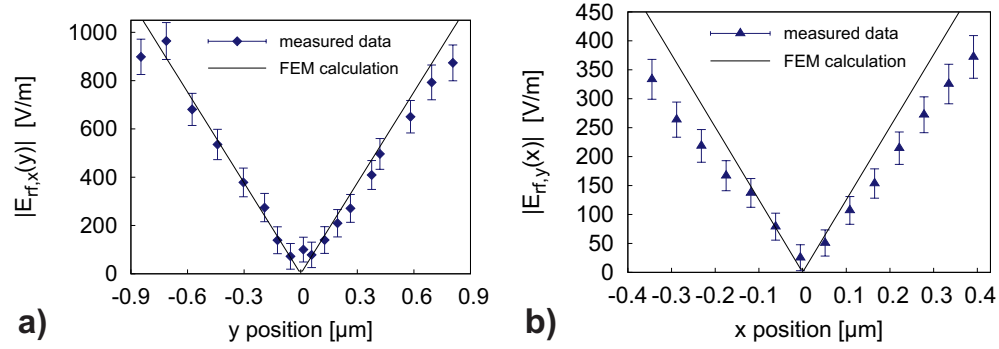


Figure 10. RF field as function of ion displacement in radial directions x and y . To check the consistency of the measured micromotion amplitudes, expected rf field amplitudes have been calculated from the measured radial secular frequencies (solid lines).

away from the rf trap boards in the center and therefore have a larger distance to the trap center in x direction. This leads to a decreased static electric field at a given compensation voltage U_{ec} . A FEM calculation, in which the distance between the compensation and trap boards is varied, shows a decrease of the dc field in x direction of about 30 % for an increase of the electrode distance of 0.25 mm, which is reasonable looking at the taken pictures.

On the other hand, along the y direction the ion is shifted by applying U_{tc} on the rf ground electrodes on the quadrupole trap boards. As these electrodes are more rigidly machined from one continuous wafer and measured secular frequencies have confirmed the expected rf quadrupole geometry, no relevant deviations in the applied dc fields, created by U_{tc} , are expected here. This gives a strong argument for the good agreement between the measurement and the calculations in the case of the vertical ion shift, where $E_{\text{rf},x}$ is measured.

To measure residual axial rf fields, a single ion was shifted in the direction of the trap axis and the micromotion was measured, see figure 11. The laser beams have been adjusted while shifting the ion, in order to prevent systematic uncertainties due to a change in the intensity at the ion position. As a cross-check we measured the residual radial rf field and verified a value below 115 V/m in the range of $0 < z < 200 \mu\text{m}$.

In addition to that, FEM calculations have been carried out for comparison. The calculations include the contribution to the rf electric field due to the finite length of the trap as well as the slits between the electrodes. Alignment and machining uncertainties and their effect on the rf field have been investigated in [4]. According to that, variations in the width of the slits between the electrodes due to machining tolerances would affect the measured field gradient and can be an explanation for the slightly larger rf fields.

Besides that, we observed a deviation of $100 \mu\text{m}$ between the ion position with minimum micromotion and the average ion position for symmetric axial dc voltages $U_{\text{ax},1} = U_{\text{ax},3} = 4.0 \text{ V}$, which is at $z = 0$ in figure 11. This can be due to angular misalignment of the trap boards, leading to an offset in the axial rf field in the trapping

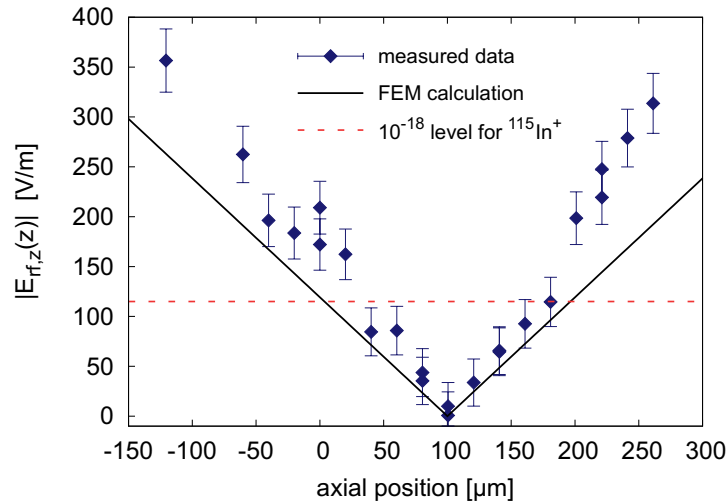


Figure 11. Residual axial rf electric field along trap axis derived from measured micromotion amplitude (diamonds) compared to axial rf field estimated from FEM calculations (solid line). The dashed line indicates the rf field, for which the relative frequency shift induced by micromotion is smaller than 10^{-18} for an indium ion optical clock. The zero axial position corresponds to the ion position for $U_{\text{ax},1} = U_{\text{ax},3} = 4 \text{ V}$, where the measurement was initiated.

region [4], machining tolerances of the electrode notches or dc stray fields, shifting the ion from their average position in the axial trapping potential. These effects are not distinguishable in the present setup.

For optical clock operation with In^+ ions, the amplitudes of axial rf fields need to be $|E_{\text{rf}}| < 115 \text{ V/m}$ to guarantee a small enough fractional frequency shift due to time dilation of $|(\Delta\nu/\nu)_{\text{mm}}| = 4E_{\text{rf}}^2 e^2 / (m^2 \Omega_{\text{rf}}^2) \leq 1 \times 10^{-18}$. We find a length of about $130 \mu\text{m}$ in our ion trap driven at an rf voltage amplitude of 810 V , within which this condition is fulfilled. At full rf amplitude of 1500 V , this length is reduced by about a factor of two, allowing space for about 12 trapped ions.

5. Conclusion

We presented a new experiment to test novel ion traps for optical clock operation with flexible optical access to perform measurements of micromotion in all dimensions. In our new scalable ion trap, we are able to load and trap single $^{172}\text{Yb}^+$ ions as a high-resolution electric field probe, as well as linear Coulomb crystals for multi-ion optical clock operation. We detailed on the design and construction of a novel ion trap based on stacked printed circuit boards with on-board filter electronics and a low loss rf circuit with a loaded quality factor of $Q_{\text{loaded}} = 640$. Using photon-correlation spectroscopy we demonstrated the measurement of fractional frequency shifts due to excess micromotion with a resolution of $< 10^{-19}$, which allows us to characterize trap designs for the use of an optical clock with lowest systematic shifts.

With this, we were able to show that already the printed circuit board trap features

a region of $130\text{ }\mu\text{m}$ along the trap axis, in which the relative frequency shift due to micromotion is $|(\Delta\nu/\nu)_{\text{mm}}| \leq 1 \times 10^{-18}$ at a trap voltage of $U_{\text{rf}} = 810\text{ V}$. For a multi-ion clock based on $^{115}\text{In}^+$ ions, this corresponds to a region of $70\text{ }\mu\text{m}$ operating the ion trap at $U_{\text{rf}} = 1500\text{ V}$ and $\omega_{\text{In,rad}} = 2\pi \times 1.5\text{ MHz}$, $\omega_{\text{In,ax}} = 2\pi \times 225\text{ kHz}$. This allows to trap a chain of about 12 $^{115}\text{In}^+$ ions for optical clock operation with $|(\Delta\nu/\nu)_{\text{mm}}| \leq 10^{-18}$.

Based on the design presented and tested in this paper, an ion trap of laser-cut AlN wafers will be machined in-house. Here, a better mechanical stiffness and precision can be obtained and only non-magnetic materials will be used. We expect an improvement in the performance in terms of axial micromotion as well as heat conductivity for precise ion trap temperature evaluation. In addition, a larger number of trap segments will allow to increase the number of ions used for spectroscopy.

Acknowledgments

We thank Max Harlander and Yves Colombe for exchanging experience on low outgassing components, Christian Tamm for discussions on detection optics and trap electronics and trap electronics and Kihwan Kim for providing us with SMD parts for preliminary tests. We thank Ekkehard Peik and Kristijan Kuhlmann for a careful reading of this manuscript. This work was supported by the cluster of excellence QUEST.

References

- [1] Chou C W, Hume D B, Koelemeij J C J, Wineland D J and Rosenband T 2010 Frequency comparison of two high-accuracy Al^+ optical clocks *Phys. Rev. Lett.* **104** 070802
- [2] Schmidt P O, Rosenband T, Langer C, Itano W M, Bergquist J C and Wineland D J 2005 Spectroscopy using quantum logic *Science* **309** 749–752
- [3] Roberts M, Taylor P, Barwood G P, Gill P, Klein H A and Rowley W R C 1997 Observation of an electric octupole transition in a single ion *Phys. Rev. Lett.* **78** 1876–1879
- [4] Herschbach N, Pyka K, Keller J and Mehlstäubler T E 2011 Linear Paul trap design for an optical clock with Coulomb crystals *Appl. Phys. B* DOI 10.1007/s00340-011-4790-y
- [5] Champenois C, Marciante M, Pedregosa-Gutierrez J, Houssin M, Knoop M and Kajita M 2010 Ion ring in a linear multipole trap for optical frequency metrology *Phys. Rev. A* **81** 043410
- [6] Madsen M J, Hensinger W K, Stick D, Rabchuk J A and Monroe C 2004 Planar ion trap geometry for microfabrication *Appl. Phys. B* **78** 639–651
- [7] Home J P and Steane A M 2006 Electrode configurations for fast separation of trapped ions *Quantum Inform. Comput.* **6** 5
- [8] Stick D, Hensinger W K, Olmschenk S, Madsen M J, Schwab K and Monroe C 2006 Ion trap in a semiconductor chip *Nat. Phys.* **2** 36–39
- [9] Schulz S, Poschinger U, Singer K and F Schmidt-Kaler F 2006 Optimization of segmented linear Paul traps and transport of stored particles *Fortschr. Phys.* **54** 648–665
- [10] Hensinger W K, Olmschenk S, Stick D, Hucul D, Yeo M, Acton M, Deslauriers L, Rabchuk J and Monroe C 2006 T-junction ion trap array for two-dimensional ion shuttling, storage and manipulation *Appl. Phys. Lett.* **88** 034101
- [11] Leibrandt D R *et al* 2009 Demonstration of a scalable, multiplexed ion trap for quantum information processing *Quantum Inform. Comput.* **9** 11

- [12] Tanaka U, Naka R, Iwata F, Ujimarui T, Brown K R, Chuang I L and Urabe S 2009 Design and characterization of a planar trap *J. Phys. B At. Mol. Opt. Phys.* **42** 154006
- [13] Pearson C E, Leibbrandt D R, Bakr W S, Mallard W J, Brown K R and Chuang I L 2006 Experimental investigation of planar ion traps *Phys. Rev. A* **73** 032307
- [14] Allcock D T C *et al* 2011 Heating rate and electrode charging measurements in a scalable, microfabricated, surface-electrode ion trap *Appl. Phys. B* DOI 10.1007/s00340-011-4788-5
- [15] Turchette Q A *et al* 2000 Heating of trapped ions from the quantum ground state *Phys. Rev. A* **61** 063418
- [16] Daniilidis N, Narayanan S, Möller S A, Clark R, Lee T E, Leek P J, Wallraff A, Schulz S, Schmidt-Kaler F and Häffner H 2011 Fabrication and heating rate study of microscopic surface electrode ion traps *New J. Phys.* **13** 013032
- [17] Schauer M M, Danielson J R, Nguyen A T, Wang L B, Zhao X and Torgerson J R 2009 Collisional population transfer in trapped Yb^+ ions *Phys. Rev. A* **79** 062705
- [18] Fawcett B C and Wilson M 1991 Computed Oscillator Strengths, and Landé g-Values, and lifetimes in Yb II *Atom. Data and Nucl. Data Tables* **47** 241
- [19] Das D, Barthwal S, Banerjee A and Natarajan V 2005 Absolute frequency measurements in Yb with 0.08 ppb uncertainty: isotope shifts and hyperfine structure in the 399-nm $^1S_0 \rightarrow ^1P_1$ line *Phys. Rev. A* **72** 032506
- [20] Macalpine W W and Schildknecht R O 1959 Coaxial resonators with helical inner conductor *Proc. of the IRE* 2099
- [21] Schrama C A, Peik E, Smith W W and Walther H 1993 Novel miniature ion traps *Opt. Comm.* **101** 32–36
- [22] Berkeland D J, Miller J D, Bergquist J C, Itano W M and Wineland D J 1998 Minimization of ion micromotion in a Paul trap *J. Appl. Phys.* **83** 5025–5033
- [23] Peik E 1993 Spektroskopie an gespeicherten In-Ionen *PhD Thesis* Max-Planck-Institut für Quantenoptik, München